JOURNAL OF GEOPHYSICAL RESEARCH, VOL. 100, NO. A9, PAGES 17,299–17,308, SEPTEMBER 1, 1995

Atmospheric Response in Aurora experiment: Observations of *E* and *F* region neutral winds in a region of postmidnight diffuse aurora

M. F. Larsen, [1] T. R. Marshall,[1] I. S. Mikkelsen,[2] B. A. Emery,[3] A. Christensen,[4] D. Kayser,[4] J. Hecht,[4] L. Lyons,[4] and R. Walterscheid[4]

Abstract. The goal of the Atmospheric Response in Aurora (ARIA) experiment carried out at Poker Flat, Alaska, on March 3, 1992, was to determine the response of the neutral atmosphere to the long-lived, large-scale forcing that is characteristic of the diffuse aurora in the postmidnight sector. A combination of chemical release rocket wind measurements, instrumented rocket composition measurements, and ground-based optical measurements were used to characterize the response of the neutral atmosphere. The rocket measurements were made at the end of a 90-min period of strong Joule heating. We focus on the neutral wind measurements made with the rocket. The forcing was determined by running the assimilated mapping of ionospheric electrodynamics (AMIE) analysis procedure developed at the National Center for Atmospheric Research. The winds expected at the latitude and longitude of the experiment were calculated using the spectral thermospheric general circulation model developed at the Danish Meteorological Institute. Comparisons of the observations and the model suggest that the neutral winds responded strongly in two height ranges. An eastward wind perturbation of ~100 m s^{-1} developed between 140 and 200 km altitude with a peak near 160 km. A southwestward wind with peak magnitude of ~150 m s^{-1} developed near 115 km altitude. The large amplitude winds at the lower altitude are particularly surprising. They appear to be associated with the upward propagating semidiurnal tide. However, the amplitude is much larger than predicted by any of the tidal models, and the shear found just below the peak in the winds was nominally unstable with a Richardson number of ~0.08.

Introduction

One of the goals of the Atmospheric Response in Aurora (ARIA) experiment was to measure the response of the neutral atmospheric circulation and composition to a heating event on the dawnside of the auroral oval. Simulations by *Walterscheid et al.* [1985] and *Lyons and Walterscheid* [1986] have suggested that the response of the neutral atmosphere will be especially strong in the region of diffuse aurora characteristic of the morning side. In particular, the broad spatial extent and the long-lived nature of the diffuse aurora are expected to produce Lorentz forcing and Joule heating over a broad region for an extended period. The discrete aurora which typically characterize the duskside may produce stronger local forcing, but the response of the neutrals will be more limited since the spatial extent of the forcing region is small enough that the neutrals pass through the heating and acceleration regions quickly.

Over the years, there have been numerous measurements of the *F* region neutral flow on the dawn side of the auroral oval. The Dynamics Explorer observations are probably the most extensive [see, *Killeen et al.*, 1986]. However, the number of *E* region measurements has been limited in part due to the difficulty of making neutral wind measurements in that height range. Furthermore, we are not aware of any extensive analysis of the response of the *E* region neutral atmosphere to a heating event associated with diffuse aurora in the postmidnight sector.

The specific objective of the ARIA experiment was to measure the winds and composition in the postmidnight sector following a heating event lasting at least 60-90 min. To this end, the chemical release technique was used to measure the winds over an extended height

[1]Department of Physics, Clemson University, Clemson, South Carolina.
[2]Division of Geophysics, Meteorological Institute, Copenhagen, Denmark.
[3]National Center for Atmospheric Research, Boulder, Colorado.
[4]The Aerospace Corporation, Los Angeles, California.

Paper number 95JA01346.
0148-0227/95/95JA-01346$05.00

range in the mesosphere and lower thermosphere, and an instrumented rocket was used to measure the neutral composition and particle energies. In addition, an extensive set of ground-based instrumentation provided measurements of the magnetic fields and electron energies throughout the night. In this article, we will focus on the neutral wind measurements made with the chemical release rocket technique.

Geophysical Conditions

The chemical release experiment took place on March 3, 1992. The launch followed a period of approximately 90 min of local heating in the Alaska sector. The three-hourly *Kp* values for the period beginning on February 24 and ending on March 6 are shown in Figure 1. The period is characterized by higher activity levels prior to March 1 and lower activity levels during the period from March 1-6. The release on March 3 took place at 1404 UT. The *Kp* values prior to the launch were 3^+ and 3. The slightly elevated values were associated with the localized heating event which will be described below. The *Kp* values before and after the heating event were 2^-.

Interplanetary Magnetic Field

Interplanetary magnetic field (IMF) measurements were available from the IMP 8 satellite for the period from February 26 to March 6, i.e., for a period beginning approximately 6 days prior to the launch. The measurements are not presented here but show that the predominant trends were that B_z was close to zero on February 26 and 27, positive on February 28, variable on February 29 and March 1, and generally negative for the period from March 2 to March 3. B_y was generally positive throughout the period with the exception of February 26 when the component was negative and a period on February 29 when the sign was variable.

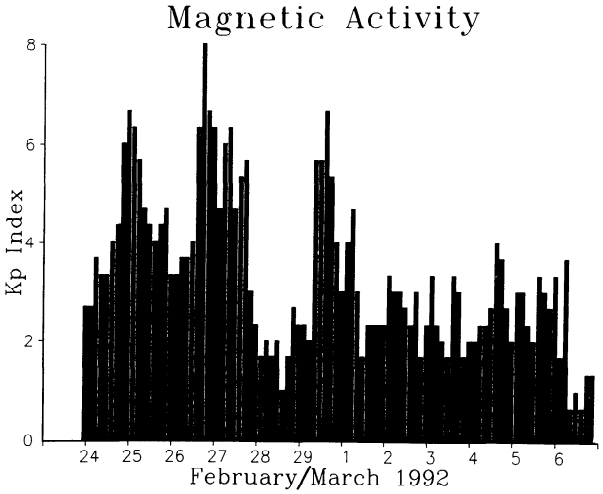

Figure 1. *Kp* indices for the period from February 24 to March 6, 1992. The chemical release experiment occurred on March 3 at 1400 UT.

The general trends in the IMF were used to specify the plasma convection pattern which provides the magnetospheric forcing in the spectral thermospheric general circulation model run which will be described later.

Magnetometer Data

Magnetometer data for the entire period of interest were available from the Alaska chain. The magnetometer traces for March 3 are shown in the article by *Anderson et al.* [1995]. The College magnetometer located at 64.46°N, 257.42°E clearly shows the heating event that preceded the rocket launches. Prior to 1000 UT, there was little activity. At approximately 1000 UT, the H component in particular shows the beginning of the disturbance. The maximum deviation at College was close to 500 γ with smaller deviations of $\sim$ 250 γ at the other two stations. The Z and H components at Arctic Village (67.94°N, 255.54°E) were comparable while the Poker Flat magnetometer measurements (64.95°N, 257.54°E) indicated almost no Z component. The Fort Yukon (66.69°N, 257.74°E) values were intermediate. All the station locations are given in terms of the geomagnetic coordinates. The combination of the three magnetometer traces indicates that the maximum electrojet current was located closest to Poker Flat. The total duration of the period of significant local heating was close to 2 hours. The chemical release and instrumented rocket launches took place just after 1400 UT. The downleg measurements of the instrumented rocket and the location of the release correspond to a location between Fort Yukon and Arctic Village, i.e., north of the maximum heating region at the time of the launch. An interesting feature of the magnetometer data is that the Fort Yukon values are slightly smaller than either the College or Arctic Village values, indicating that there was a local minimum in the heating north of the launch site. The detailed characteristics of the substorm are described in the article by *Anderson et al.* [1995].

Plasma Drifts and Joule Heating Estimates

Since the goal of the experiment was to determine the response of the neutral atmosphere to Joule heating, obtaining estimates of the electric field magnitudes and directions was critical. The available information included the magnetometer data already discussed in the previous section and some DMSP satellite measurements of the plasma drifts across the auroral oval/polar cap region. In order to make the best use of the available measurements, the assimilated mapping of ionospheric electrodynamics (AMIE) procedure developed at NCAR was used to assimilate the various types of data in order to produce estimates of the required parameters that are consistent with all the measurements. The details of the AMIE model, which is based on the techniques developed by *Richmond and Kamide* [1988], have been described by *Knipp et al.* [1989]. Empirical models provide a first guess that is modified by the observations. In that way, missing values are interpolated or estimated from empirical model output. The

result is that both the temporal and spatial variations of the plasma convection, conductivities, and Joule heating can be obtained.

The input to the AMIE analysis included the data from the Alaska magnetometer chain, stations in the Canadian sector, and those in the Greenland chain. The DMSP satellite data were provided by R. Heelis of the University of Texas at Dallas. Conjugacy was assumed so that satellite measurements in the southern hemisphere could be used for the northern hemisphere analysis. Finally, the IMP 8 satellite measurements of the interplanetary magnetic field and the *Kp* values were used as input to the empirical models.

The electric potential and Joule heating estimates within the polar cap/auroral oval region derived from the AMIE analysis are shown by *Anderson et al.* [1995] for 1300 UT. The launch site at Poker Flat is at 65°N, and the chemical release occurred close to 67°N latitude. The local time in the Alaska sector is 9 hours earlier, and the magnetic local time is approximately 10.5 hours earlier than universal time. The Alaska sector therefore was near 0230 MLT at 1300 UT, which was near the time of the maximum heating. An area of weak heating was evident on the duskside of the auroral oval, but the strongest heating was highly localized on the dawnside between 0000 and 0500 MLT.

Figure 2 shows the eastward plasma drift from the AMIE analysis as a function of latitude along the magnetic meridian through the Alaska sector. The velocity components are in invariant coordinates. The top frame is at 1200 UT. Subsequent frames are separated by 30 min so that the bottom frame corresponds to 1400 UT, close to the time of the launch. The location of the release is shown by the arrow in the bottom panel. Throughout the 2.5-hour period, the region of maximum eastward plasma flow moved northward. The maximum drifts occurred near 1300 UT with magnitudes of ~800 m s^{-1}. The northward drifts were small and are not shown.

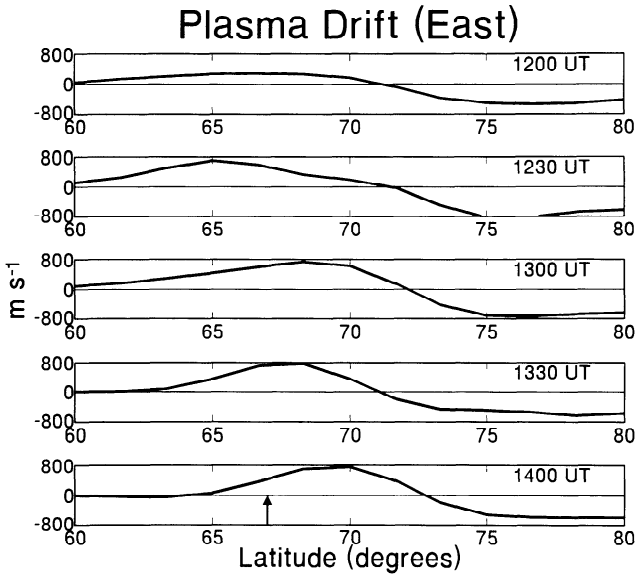

Figure 2. Eastward plasma drift component as a function of latitude for the magnetic meridian through the Alaska sector. The top panel corresponds to 1200 UT. Subsequent panels are separated by 30 min. The arrow in the bottom panel indicates the latitude of the chemical release measurement.

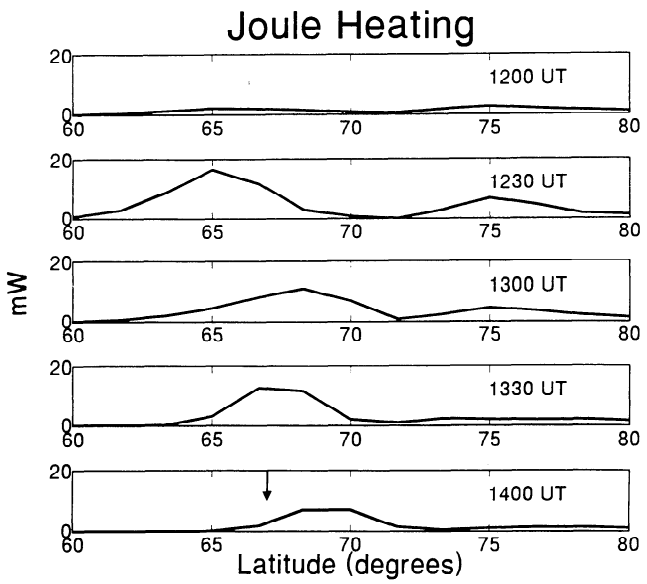

Figure 3. Joule heating in a format similar to that used in Figure 2. The values were obtained from the assimilated mapping of ionospheric electrodynamics (AMIE) analysis.

The Joule heating estimates in a similar format are shown in Figure 3. There was little heating at 1200 UT. The maximum values occurred at 1230 and 1300 UT. Note that there were two local maxima in the heating rates. At 1300 UT, one of the maxima was located near 68°N and the other was located near 75°N. These results are consistent with the inferences drawn directly from the magnetometer data. As time increased, the northern maximum diminished and the southern maximum moved north and decreased in intensity. Figure 3 in particular shows that the local heating had diminished considerably at the time and position of the release, although the same region had been subjected to the maximum heating rates associated with the event over the one-hour period prior to the release.

Anderson et al. [1995] have improved the local Joule heating estimates based on the optical and instrumented rocket observations described in their article. The results indicate that the AMIE procedure probably underestimated the heating somewhat since the electron densities in the model calculation were too low.

Instrumented Rocket Data

The instrumented rocket measurements provided extensive composition and particle energy measurements which are described in detail in the companion papers by *Anderson et al.* [1995] and *Hecht et al.* [1995]. However, the electron density measurements are of particu-

lar interest for the interpretation of the wind measurements and will also be described here. The profiles are shown in Figure 4. The profiles obtained for both the upleg and downleg portion of the flight have been plotted. The densities were much greater on the upleg with a maximum approaching 4×10^5 cm^{-3} near 105 km. The peak densities on the downleg were almost an order of magnitude less. Peak values occurred near 115 km.

Wind Measurements

The neutral winds in the E and F regions were measured by the chemical release technique to obtain a detailed profile of the winds from approximately 90 to 190 km after the period of strong Joule heating. The chemical release experiment consisted of a 12 kg trimethyl aluminate (TMA) trail released on the downleg portion of the trajectory of a Nike-Tomahawk sounding rocket launched at 1357 UT from the Poker Flat Research Range. The launch azimuth was 5° east of north. The range to impact was approximately 250 km, and the trail was released between heights of 190 and 90 km. The release was initiated at 1404 UT, and the total flight time was approximately 10 min.

Since the release started at 0404 LT, none of the trail was illuminated by sunlight so that the release was only visible because of the chemiluminescence of the TMA which reacts with oxygen. The trail was visible for almost ten minutes, a period which is more than adequate for triangulation with good accuracy. The trail was photographed from sites located at the rocket range, at Arctic Village, and at Cold Foot. The triangulation is carried out by digitizing the star and trail positions on photographs taken simultaneously at the three sites. Triangulation software is then used to carry out a least squares fit of photographed and known star positions

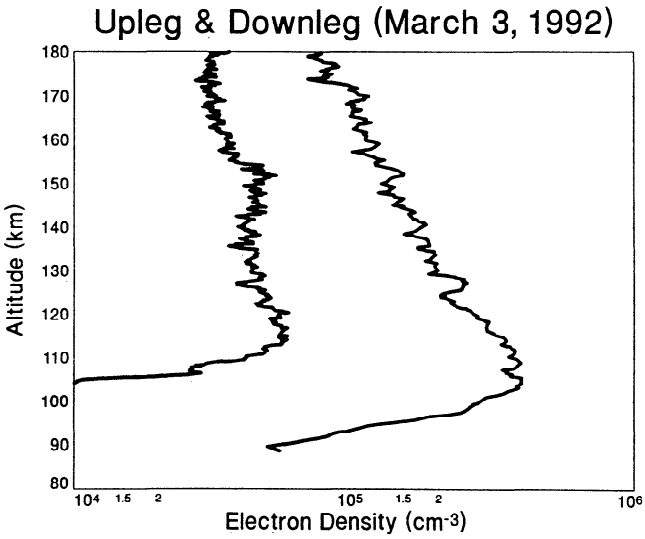

Figure 4. Electron density profile obtained from the instrumented rocket measurements. Both the upleg and downleg profiles are shown. The upleg profile is characterized by much larger electron densities.

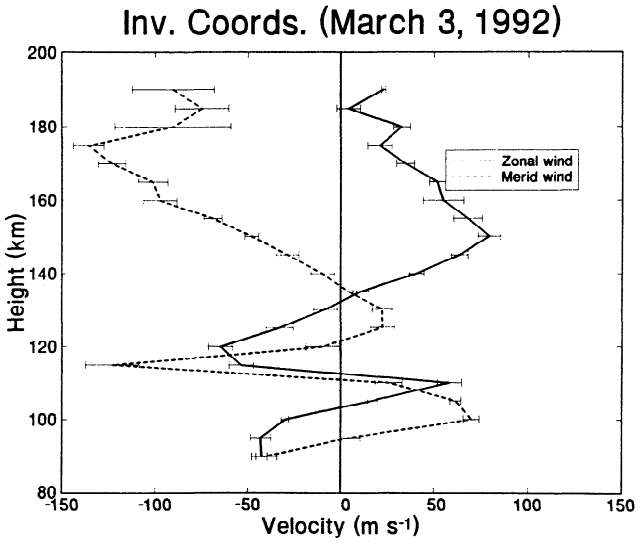

Figure 5. Wind profile measured with the chemical release technique at 1400 UT on March 3, 1992. The wind components have been rotated to correspond to magnetic coordinates. The dashed line shows the meridional wind profile. The solid line shows the zonal wind component.

obtained from a computer star atlas. The least squares fitting eliminates lens aberration effects and creates a mapping of the photograph coordinates to line-of-sight directions from the observing position. Next, the software calculates the intersection positions for portions of the trail observed from the three locations. The change in position with time gives the velocity. The error in the position for a given triangulation is determined from the minimum separation between the lines-of-sight from either two or three differenct locations. Ideally, the lines-of-sight should intersect but generally do not due to errors in the digitizing procedure or in the determination of the midpoint of the trail at a given altitude. The uncertainty in the velocity determination is based on the closest approach values for the individual position determinations. Typical uncertainties are in the range of 5-10 m s^{-1}.

The wind profile obtained from the TMA release is shown in Figure 5. The wind components are shown in a coordinate system that has been rotated by 30° toward the east to correspond to invariant coordinates. The plasma drifts from the AMIE analysis shown earlier have also been calculated in invariant coordinates. The uncertainties are plotted as error bars for each height. An eastward wind is evident at the upper altitudes with a peak near 150 km. At 180 km, the wind has turned toward south. Another significant feature is the large wind maximum near 115-km altitude. The wind speed is almost 150 m s^{-1}, and the direction is toward south-southeast. The shear below the wind maximum exceeds 150 m s^{-1} over a height range of just 2.5 km. The Richardson number associated with the shear can be estimated by combining the measured winds with the temperature profile predicted by MSIS-86 [*Hedin*, 1987]

in order to estimate the Brunt-Vaisala frequency. The resulting value is ~0.08, i.e., significantly less than the critical value for instability of 0.25.

The study by *Johnson et al.* [1987] represents one of the few extended set of wind measurements from the lower E region. Their analysis was based on incoherent scatter radar data obtained with the instrument that was located at Chatanika, a few miles from the Poker Flat Research range. Most of their results deal with wind averages and tidal component decomposition, but they also present the wind measurements at 115 km altitude for a disturbed day on June 11, 1980. Their analysis shows very large southward winds developing in the postmidnight sector in response to the disturbed conditions with wind speeds in excess of 200 m s^{-1} at 115 km near 1400 UT. Their results are thus similar to ours but show even larger wind speeds.

The hodograph for the same wind profile is shown in Figure 6. The numbers next to the curve indicate the corresponding altitudes. Once again, the wind maximum is toward southsoutheast. The large wind shear below the maximum, and the rotation of the wind direction with height is evident.

Comparisons With Spectral Thermospheric General Circulation Model Simulations

The wind measurements are difficult to interpret in isolation. The profile shown in Figure 5 has considerable structure throughout the height range of the measurements. The most noticeable feature of the wind profile is the wind maximum at 115-km altitude. The high-speed flow is localized in height with a characteristic vertical scale of only 2.5-5.0 km. The dynamical processes responsible for the jet are not clear. The rotation of the wind vector with height is generally consistent with the expected behavior of the semidiurnal tide. However, the vertical wavelength near 115 km is much shorter, and the wind speed is much greater than theoretical predictions. In order to clarify the dynamics responsible for the observed wind profile features, we have used the spectral thermospheric general circulation model (STGCM) which has been developed at the Danish Meteorological Institute [*Mikkelsen and Larsen*, 1991, 1993].

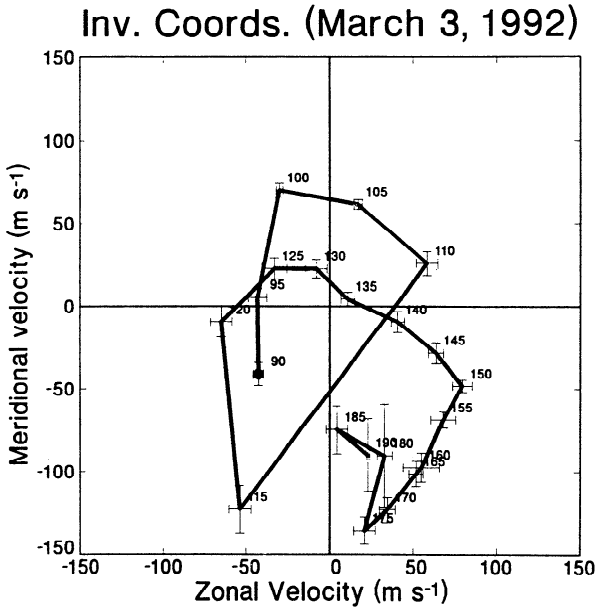

Figure 6. Hodograph showing the wind variation with height for the same data as in Figure 5. Magnetic coordinates are also used in this plot. The small numbers next to the curve show the corresponding heights.

We showed earlier in a number of comparisons between the model results and previous chemical release wind measurements [*Mikkelsen and Larsen*, 1993] that the model can produce winds that are in reasonable agreement with the measurements, particularly when a detailed history of the forcing over a period of several days prior to the measurements is used in the model run. In this case, we started the simulation eight days prior to the time of the measurements and used the general trends in the IMP 8 IMF measurements described earlier and the Kp values to specify the forcing. The IMF values define the convection pattern, and Kp determines the characteristics of the auroral ionization. A detailed description of the model and the specification of the forcing has been given in the earlier papers cited above.

The model circulation at 1400 UT on March 3 is shown in Figures 7 and 8. Figure 7 represents the flow pattern at 198 km and 179 km altitude as a function of local time and geographic latitude. The heavier solid lines are the stream function contours. The lighter solid lines are the velocity potential contours. The flow velocity is proportional to the spacing between adjacent contours. The scales in the upper lefthand corner of each frame can be used to convert the contour spacing to wind speed. The rotational wind component is dominant, so the flow is approximately parallel to the stream function contours. The pattern shows a large dusk vortex with high flow velocity and a weaker and much smaller dawn vortex. The position of the magnetic pole is indicated by "M" in Figure 7. The location of the measurements is indicated by an "A." The simulations show that the flow around 180 km altitude is associated with the outflow from the polar cap produced by the antisunward convection. The direction of the predicted flow is consistent with the measured flow direction at those altitudes.

Figure 8 shows the simulated flow at 119 and 113 km altitude in the same format. The circulation at 119 km is characterized by both a dawn and a dusk cell, although the centers of the two vortices have rotated considerably with height so that the continuation of the dawn cell is actually on the duskside. A similar rotation with height has been noted in a number of earlier modeling studies. The location of Alaska within the flow at those two heights is in the region characterized by tidal flow oscillations. The tidal component can be distinguished by the four-lobe pattern which is particularly

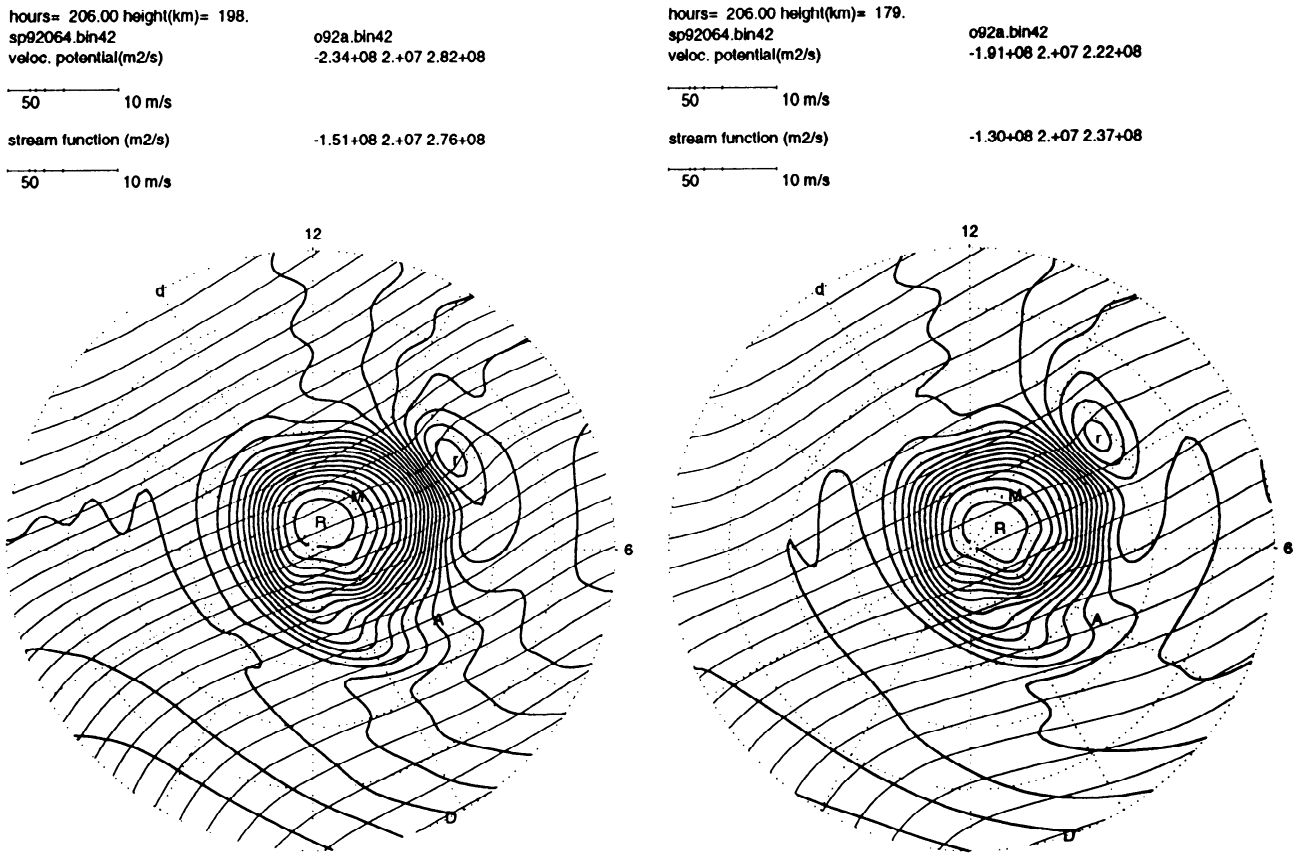

Figure 7. Stream function and velocity potentials from the spectral thermospheric general circulation model simulations for heights of 198 and 179 km at the time of the chemical release wind measurements. The flow velocities increase with decreasing separation between the contours. Velocity scales appear at the top.

evident in the velocity potential contours but can also be distinguished in the stream function contours which are 90° out of phase. Thus the model run suggests that any structure observed in the wind profile in the lower E region should be associated with the upward propagating tides. We will examine that possibility in more detail in the next section. The amplitude and phase of the tides used to force the lower boundary in the model were taken from the article by *Forbes and Vial* [1990].

In Figure 9, we have plotted the STGCM winds for altitudes of 250 and 120 km to correspond approximately to heights representative of the F region and E region neutral flow. The F region winds are generally northward prior to 1100 UT with a shift to southward winds after that time. At the time of the chemical release measurements, both the model and the measurements show winds toward the southsouthwest, although the model winds are smaller in magnitude than the observations.

The agreement between the 120-km model winds and the observed winds is much poorer. As shown by the stream function and velocity potential contours in Figure 8, the model predicts a flow that is dominated by the upward propagating tides in the lower thermosphere at the location of the observations. The 120-km winds in Figure 9 show a variation that is characteristic of the wind pattern produced by the tides. The maximum northward wind occurs near 1100 UT. The maximum southward wind component occurs at 0500 UT, i.e., 6 hours earlier and consistent with the the semidiurnal tide.

The chemical release wind profile shows large vertical shear in both the direction and wind speed between 105 and 115 km. The wind direction reverses and the velocity changes by more than 150 m s^{-1}. The shear in the model winds is not nearly as great but is also significant. Figure 10 shows the model wind hodographs at five positions near the latitude and longitude of the release. The numbers at the top of each frame are the heights of the discrete isobaric levels used in the model. The symbols used to mark the heights in the hodographs are shown below the corresponding heights. The loops at the lower heights are characteristic of the tidal variations, but above 117 km, indicated by the square symbol, the wind variation is approximately linear, i.e., there is shear in the magnitude but not in the direction.

Finally, we show the wind profile obtained from the model simulations in the same format as the measured chemical release wind profile. The curves are shown in Figure 11. The agreement is reasonable above 140 km altitude, but there is significant disagreement below 140 km. The model does not show the 150 m s^{-1} southward winds evident in the chemical release measurements. As

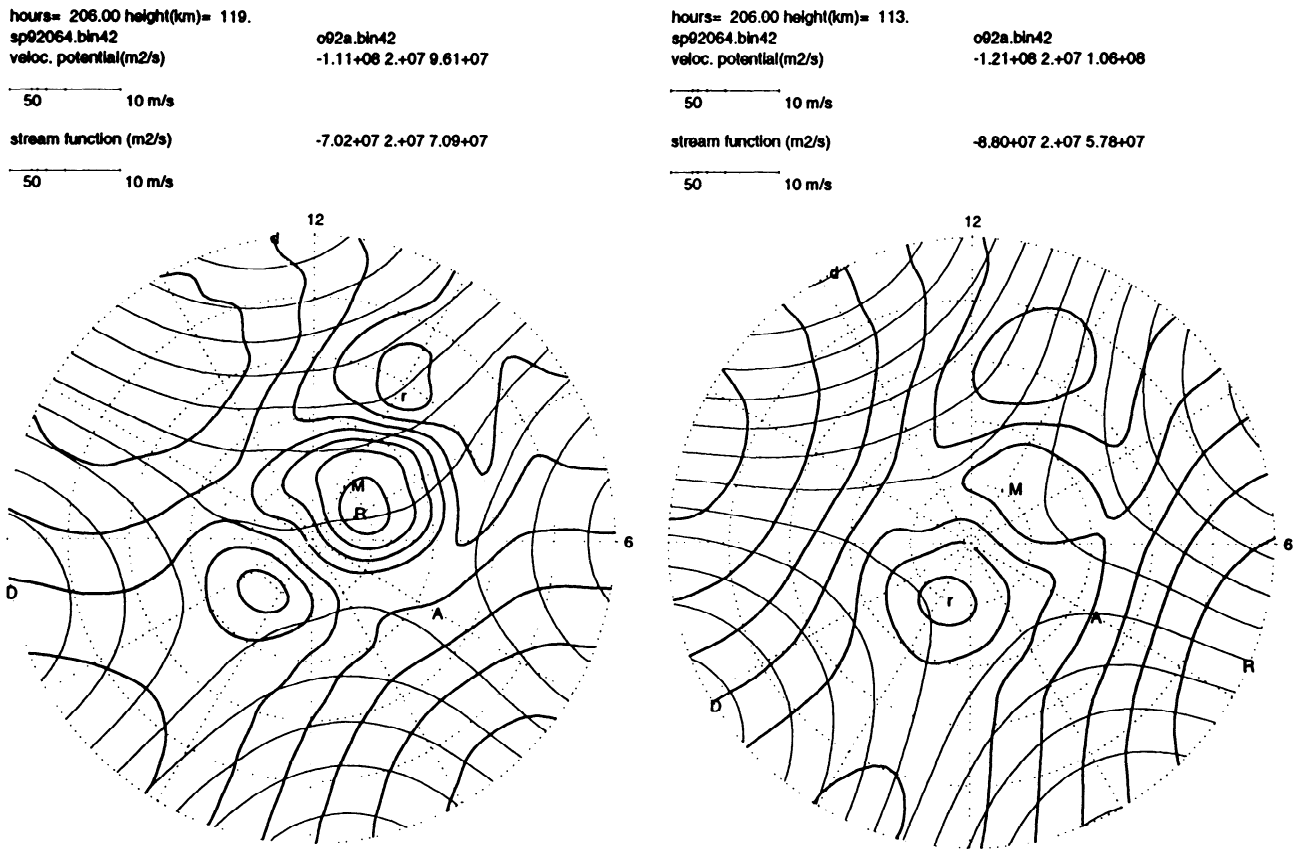

Figure 8. Similar to Figure 7 but for heights of 119 and 113 km.

the chemical trail measurements show, the feature was extremely narrow with a vertical scale of only 2.5-5.0 km near the peak in the wind profile.

Conclusions

Response to Lorentz Forcing/Joule Heating

The difference between the model-predicted winds and the observed winds can be interpreted as being due to the localized forcing which the model does not include. The comparisons show that an eastward wind was produced above approximately 140 km altitude. The magnitude of the induced wind was close to 100 m s^{-1}, much less than the values predicted by the *Walterscheid et al.* [1985] model. However, the observed eastward winds were measured above the height range where the maximum winds would be expected based on the simulations [see, *Brinkman et al.*, 1995]. The specific response will depend on the history of the forcing over a period of several hours prior to the release.

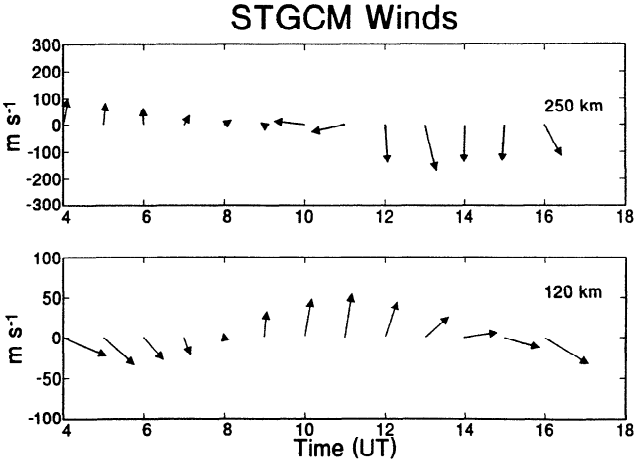

Figure 9. Vector winds at Poker Flat obtained from the spectral thermospheric general circulation model run. Winds at 250 and 120 km are shown as a function of universal time.

Large-Amplitude Winds in the Lower E Region

The source of the large winds observed near 115 km is not clear. The wind rotation with height is in agreement with the expectations for a semidiurnal tidal oscillation. However, the wind speed magnitude in excess of 150 m s^{-1} is considerably larger than theoretical predictions for that height range. Also, the vertical wavelength is much smaller than predicted by theory. The possibility exists that the structure is produced by a breaking tide. Some credence is lent to the latter idea by the fact that the Richardson number associated with the bottomside shear is estimated to be less than 0.1. The fact that the vertical wavelength is small is also consistent with the breaking wave hypothesis. The vertical structure and wind direction is clearly not consistent with the results from the STGCM model run which includes the tidal forcing at the lower boundary. In particular, the

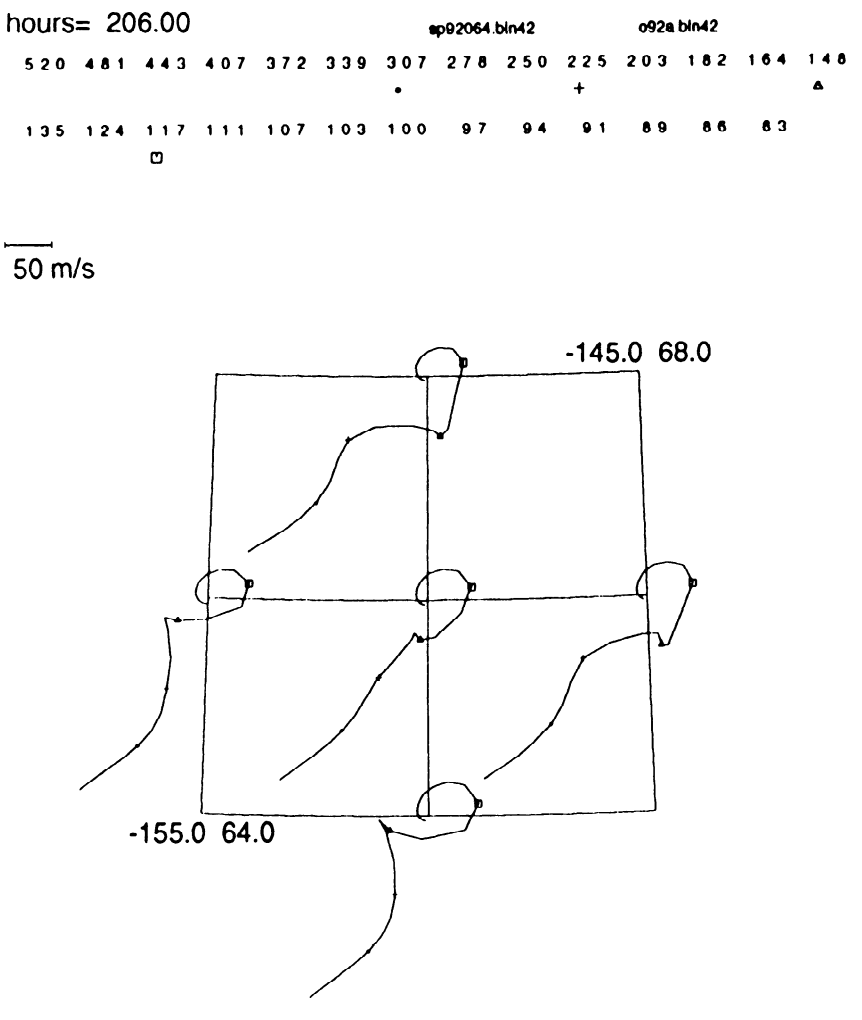

Figure 10. Wind hodographs from the model at 1400 and 1500 UT. The curves at four positions surrounding the observations are shown.

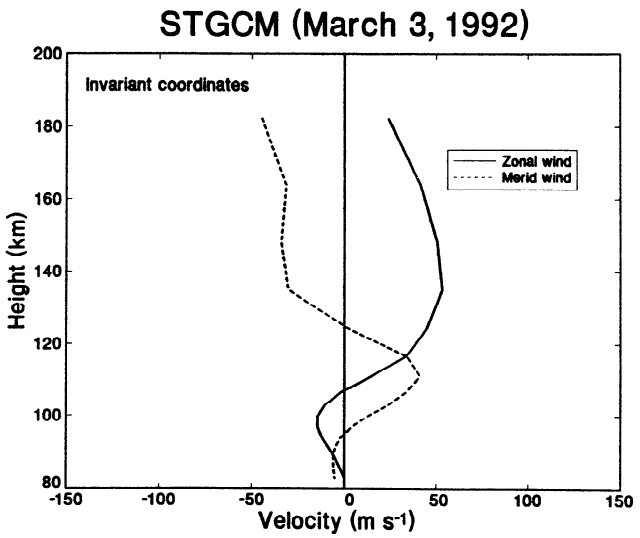

Figure 11. Model wind profile for 1400 UT at the location of the release. The wind components have been rotated to correspond to magnetic coordinates.

phase of the tidal component used to force the lower boundary has to be in error if the observed structure is associated with a tidal component. Since the tidal phases are known to vary significantly from day to day, the latter is a distinct possibility.

Can the structure near 115 km be produced entirely by Joule heating or Lorentz forcing? We have calculated the Hall and Pedersen ion drag coefficients using the MSIS-86 model and the observed upleg electron density profile derived from the instrumented rocket measurements. The results are shown in Figure 12. The Pedersen drag coefficient is small below 120 km, but the Hall drag peaks between 115 and 120 km altitude. The magnitude of the coefficient is $\sim 9\times10^{-5}$ s^{-1} which implies an acceleration time constant of $\sim$ 3 hours. For a dominant Pedersen drag, the neutral flow should be roughly in the same diretion as the plasma drift, i.e., eastward in this case. However, the response to a dominant Hall drag is more complicated and can produce a flow directed antiparallel to or at right angles to the F region plasma drift direction, as discussed by *Larsen and Walterscheid* [this issue], who considered a balanced flow described by the two momentum equations which apply in the thermosphere, namely,

$$\frac{du}{dt} = -\frac{\partial\Phi}{\partial x} + (f-\beta^*)v + \beta^* v_p + \alpha^*(u_p - u) \quad (1)$$

$$\frac{dv}{dt} = -\frac{\partial\Phi}{\partial y} + -(f-\beta^*)u - \beta^* u_p + \alpha^*(v_p - v) \quad (2)$$

where u and v are the eastward and westward components of the horizontal velocity, respectively. The electric field appears in the equations implicitly, although it is written in terms of the F region $\mathbf{E}\times\mathbf{B}$ plasma flow velocity components u_p and v_p. The plasma drift velocity components, and the electric fields which drive them, are momentum source terms in the equations. The other terms include the Coriolis parameter f, the Pedersen drag α^*, and the Hall drag term β^*. The first terms on the right-hand side of the two equations are the geopotential gradient components which are equivalent to the pressure gradient terms. Since f only appears as a difference with β^*, we can equivalently consider a flow characterized by a modified Coriolis parameter which is reduced by the magnitude of the Hall drag coefficient. *Larsen and Walterscheid* [this issue] have shown that, in the limiting case of steady state flow with $\beta^* >> \alpha^*$ and a plasma drift velocity that is much greater than the geostrophic wind corresponding to the geopotential gradient, the solution for the zonal wind component u reduces to

$$u \sim -\frac{\beta}{1-\beta}u_p \quad (3)$$

where β is the Hall drag coefficient made dimensionless by dividing by f. Since β is positive and typically less than 1, the result shows that the effect of the Hall drag term is to increase the wind speed at heights where the Hall conductivity becomes significant. The discussion here is only sufficient to indicate the physics responsible for the effect. *Larsen and Walterscheid* [this issue] have provided a detailed derivation and justification for the result.

Their results predict that the neutral flow will rotate with decreasing height toward a direction that is approximately perpendicular to the direction of the plasma flow. Such a tendency is evident in the chemical release wind measurements. Also, a large shear is expected on the bottom side of the wind maximum near 110-120 km. Indeed, such a shear is present in the observed wind profile. For a simple exponential time dependence, forcing over a 1-hour period with a time constant of 3 hours can produce winds of $\sim$ 30% of the plasma flow velocity. The latter was estimated to be of the order of 800 m s^{-1} based on the AMIE analysis, so qualitatively we expect that winds in excess of 150 m

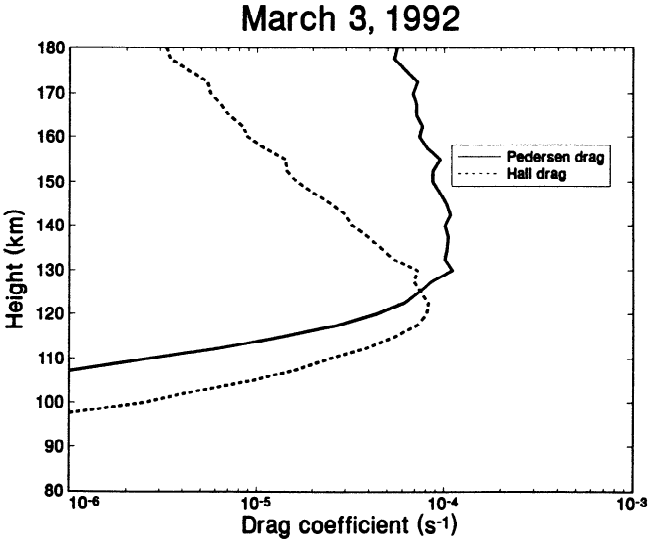

Figure 12. Profile of Pedersen and Hall drag coefficients calculated from the MSIS-86 model and the electron density profile measured by the instrumented rocket on the upleg.

s^{-1} can easily be achieved if the upleg electron density profile was indeed characteristic of the region where the release occurred during the time prior to the release. The measurements at the time of the launch showed much smaller electron densities near the location of the release, but the AMIE analysis also indicates that the forcing was decreasing at that time and that the forcing had been stronger at the position of the release during the previous hour.

A second effect related to the Hall drag which is dominant in the lower E region is related to changes in the frequency range for which vertically propagating modes are allowed in the lower E region. Ordinarily, only waves with frequencies between the Coriolis parameter f and the Brunt-Vaisala frequency will be vertically propagating. As a result, the semidiurnal tide dominates at high latitudes since the diurnal tide is not vertically propagating. The derivation by *Mikkelsen and Larsen* [1983] in their appendix leads to a dispersion relation for large-scale gravity waves that includes the effects of the Hall and Pedersen drag terms. When the drag terms are excluded, the cutoff for vertically propagating waves is $\omega = f$. However, including the drag terms modifies the cutoff frequency. The term that is most significant is the Hall drag term which directly modifies the Coriolis parameter to create an effective Coriolis parameter given by $f_{effective} = f - \beta$, where β is the Hall drag collision frequency. Changes in β with altitude can lead to regions where the diurnal tide is alternately vertically propagating and trapped. An assessment of the magnitude and significance of such effects will require more extensive analytic and modeling studies.

Although the arguments can be focused on either tides or Lorentz and Joule forcing as the source of the wind structure, a more likely explanation is that both factors influenced the observed wind profile. The tides are known to be important in that height range, but the measured electron density profiles also indicate that the Hall drag terms should have been significant in the vicinity of the measurements. Therefore the observed structure probably reflects the upward propagating tides modified by the local Hall drag and Joule heating effects.

Acknowledgments. M. F. L. was supported by NASA grants NAG5-632 and NAG5-5002 during the course of the study. T. R. M. was supported by NAG5-632. We want to thank the staff of the Poker Flat Research Range for their extremely competent help during the course of the experiment. Our thanks to Ron Lepping for providing the IMP 8 IMF measurements and to Rod Heelis of UTD for providing the DMSP satellite data.

The Editor thanks H. G. Mayr and G. Hernandez for their assistance in evaluating this paper.

References

Anderson, P. C., et al., The ARIA I rocket campaign, *J. Geophys. Res.*, in press, 1995.

Brinkman, D. G., R. L. Walterscheid, L. R. Lyons, J. R. Sharber, and M. F. Larsen, E region neutral zonal winds in the postmidnight diffuse aurora during the ARIA I rocket campaign, *J. Geophys. Res.*, in press, 1995.

Forbes, J. M., and F. Vial, Monthly simulations of the solar semidiurnal tide in the mesosphere and lower thermosphere, *J. Atmos. Terr. Phys.*, *51*, 649-661, 1989.

Hecht, J. H., A. B. Christensen, D. J. Gutierrez, W. E. Sharp, J. R. Sharber, D. J. Strickland, and D. J. McEwen, Observations of the neutral atmosphere between 100 and 200 km using ARIA rocketborne and ground-based instruments, *J. Geophys. Res.*, this issue.

Hedin, A.E., MSIS-86 thermospheric model, *J. Geophys. Res.*, *92*, 4649-4662, 1987.

Heppner, J.P., and N.C. Maynard, Empirical high-latitude electric field models, *J. Geophys. Res.*, *92*, 4467-4489, 1987.

Johnson, R.M., V. B. Wickwar, R. G. Roble, and J. G. Luhmann, Lower-thermospheric winds at high latitude: Chatanika radar observations, *Ann. Geophys., Ser. A.*, *5*, 383-404, 1987.

Killeen, T. L., et al., Mean neutral circulation in the winter polar F region, *J. Geophys. Res.*, *91*, 1633-1649, 1986.

Knipp, D. J., A. D. Richmond, G. Crowley, O. de la Beajardiere, E. Friis-Christensen, D. S. Evans, J. C. Foster, I. W. McCrea, F. J. Rich, and J. A. Waldock, Electrodynamic patterns for September 19, 1984, *J. Geophys. Res.*, *94*, 16,913-16,923, 1989.

Larsen, M. F., and R. L. Walterscheid, Modified geostrophy in the thermosphere, *J. Geophys. Res.*, this issue, 1995.

Lyons, L. R., and R. L. Walterscheid, Feedback between neutral winds and auroral arc electrodynamics, *J. Geophys. Res.*, *91*, 13,506-13,512, 1986.

Mikkelsen, I. S., and M. F. Larsen, A numerical modeling study of the interaction between the tides and the circulation forced by the high-latitude plasma convection, *J. Geophys. Res.*, *96*, 1203-1213, 1991.

Mikkelsen, I. S., and M. F. Larsen, Comparisons of spectral thermospheric general circulation model simulations and E and F region chemical release wind observations, *J. Geophys. Res.*, *98*, 3693-3709, 1993.

Rich, F. J., and N. C. Maynard, Consequences of using simple analytical functions for the high-latitude convection electric field, *J. Geophys. Res.*, *94*, 3687-3701, 1989.

Richmond, A. D., and Y. Kamide, Mapping electrodynamic features of the high-latitude ionosphere from localized observations: Technique, *J. Geophys. Res.*, *93*, 5741-5759, 1988.

Roble, R. G., and E. C. Ridley, An auroral model for the NCAR thermospheric general circulation model (TGCM), *Ann. Geophys., Ser. A*, *5*, 369-382, 1987.

Walterscheid, R. L., L. R. Lyons, and K. E. Taylor, The perturbed neutral circulation in the vicinity of a symmetric stable auroral arc, *J. Geophys. Res.*, *90*, 12,235-12,248, 1985.

A. Christensen, J. Hecht, D. Kayser, L. Lyons, and R. Walterscheid, The Aerospace Corporation, Los Angeles, CA 90009. (e-mail: andy_christensen@qmail2.aero.org)

B. A. Emery, National Center for Atmospheric Research, P. O. Box 3000, Boulder, CO 80307. (e-mail: emery@ncar.ucar.edu)

M. F. Larsen and T. R. Marshall, Department of Physics, Clemson University, Kinard Laboratory, Clemson, SC 29634-1911. (e-mail: mlarsen@hubcap.clemson.edu;)

I. S. Mikkelsen, Division of Geophysics, Danish Meteorological Institute, Lyngbyvej 100, DK-2100, Copenhagen, Denmark. (e-mail: ism@dmicvx.dmi.min.dk)

(Received April 12, 1994; revised April 25, 1995; accepted April 26, 1995.)